A&A 600, L8 (2017)
DOI: 10.1051/0004-6361/201730659

Astronomy & Astrophysics

Letter to the Editor

Extended CH_3OH maser flare excited by a bursting massive YSO

L. Moscadelli[1], A. Sanna[2], C. Goddi[3], M. C. Walmsley[1,4], R. Cesaroni[1], A. Caratti o Garatti[4], B. Stecklum[5], K. M. Menten[2], and A. Kraus[2]

[1] INAF, Osservatorio Astrofisico di Arcetri, Largo E. Fermi 5, 50125 Firenze, Italy
e-mail: mosca@arcetri.astro.it
[2] Max-Planck-Institut für Radioastronomie, Auf dem Hügel 69, 53121 Bonn, Germany
[3] Department of Astrophysics/IMAPP, Radboud University, PO Box 9010, 6500 GL Nijmegen, The Netherlands
[4] Dublin Institute for Advanced Studies, 31 Fitzwilliam Place, Dublin 2, Ireland
[5] Thüringer Landessternwarte Tautenburg, Sternwarte 5, 07778 Tautenburg, Germany

Received 20 Ferbruary 2017 / Accepted 19 March 2017

ABSTRACT

Aims. Recently, substantial flaring in the 6.7 GHz methanol maser line has been observed toward the high-mass young stellar object (YSO) S255 NIRS 3, where an accretion burst was also detected in the IR. Our goal is to study the change in the properties of the 6.7 GHz masers between the pre- and outburst phases, and investigate the connection between the maser and the accretion burst.
Methods. With the *Karl G. Jansky* Very Large Array (JVLA) and the European VLBI Network (EVN), we performed observations of the 6.7 GHz masers (covering a range in angular resolution from a few milliarcseconds to ≈1″) during the burst phase and compared these observations with pre-burst measurements at similar spatial scales.
Results. The accretion burst and the subsequent increase in IR luminosity are very likely the origin of the 6.7 GHz maser flare. Since most maser centers operate in the unsaturated regime, a change by a relatively small factor (≈5) in the flux of pumping photons has produced an exponential growth in the maser intensity. The main pre-burst maser cluster is no longer detected during the burst. Compared to the pre-burst phase, flaring 6.7 GHz masers emit across a different $V_{\rm LSR}$ range that is more strongly redshifted, and the emission extends over a larger area at larger separation from the high-mass YSO. In particular, the outburst peak emission originates from a remarkably extended (0.″2–0.″3) maser plateau at a radial distance of 500–1000 AU from the source.
Conclusions. Both the maser flare and the extraordinarily large extent of the maser structure can be a natural consequence of the burst in the accretion luminosity of the high-mass YSO. Our results strongly support models that predict IR radiative pumping for the 6.7 GHz CH_3OH masers.

Key words. ISM: kinematics and dynamics – masers – stars: formation – techniques: high angular resolution – stars: individual: S255 NIRS3

1. Introduction

The bright 5_1-6_0 A$^+$ CH_3OH maser transition at 6668.5 MHz has been recognized for a long time to be a selective signpost for recently formed luminous young stars ($L_{\rm bol} > 5\times10^3\,L_\odot$). Its excitation requires radiative pumping by 20–30 μm photons through the second torsionally excited state (Sobolev et al. 1997). Intense IR radiation typically permeates the warm dusty environment surrounding massive young stellar objects (YSO). Although the emission of most 6.7 GHz maser sources is stable on timescales of (at least) several years (Sanna et al. 2010; Moscadelli et al. 2011), in some cases, strong flares of up to several 100 Jy have been recorded. In addition, in some sources, selected maser components show a well-defined periodicity (e.g., Goedhart et al. 2004). These variations can be naturally related to an occasional and/or periodic change of the background radiation (amplified by the maser) or the IR pump field.

Recently, we have reported on the first ever detected accretion burst from a massive young star (NIRS 3) in the star-forming region S255 (Caratti O Garatti et al. 2016). This detection was triggered by the serendipitous discovery of a CH_3OH maser flare toward S255 NIRS 3 by Fujisawa et al. (2015) in 2015 November. Subsequent subarcsecond near-IR (NIR) observations showed that the K- and H-band fluxes of this source had increased with respect to the pre-burst level by 2.9 and 3.5 mag, respectively, suggesting a relationship with the maser flare (Stecklum et al. 2016). Additional IR observations proved that the integrated luminosity from NIR to millimeter wavelengths had grown from 2.9×10^4 to $1.6\times10^5\,L_\odot$ (Caratti O Garatti et al. 2016).

This letter reports on observations made with the European VLBI Network (EVN) and the Jansky Very Large Array (JVLA) of the 6.7 GHz CH_3OH maser emission in S255 NIRS 3 (hereafter NIRS 3) at the time of the outburst. We compare the new observations with previous interferometric and single-dish data, and discuss the change in the maser spatial distribution, structure, and flux.

2. Observations and data analysis

2.1. EVN 6.7 GHz CH_3OH maser

We observed the 6.7 GHz CH_3OH maser emission toward NIRS 3 with the EVN[1] as a Target of Opportunity program on

[1] The European VLBI Network is a joint facility of European, Chinese, South African and other radio astronomy institutes funded by their national research councils.

Table 1. EVN and JVLA 6.7 GHz CH_3OH maser observations.

Array	Epoch (yy/mm/dd)	HPBW (arcsec)	Δv (km s^{-1})	Image rms (mJy beam^{-1})
EVN	2004/11/06	0.006	0.09	6
EVN	2016/04/12	0.005	0.04	5
JVLA-B	2016/08/01	0.990	0.09	4
JVLA-A	2016/10/15	0.281	0.09	2

Notes. Columns 1 and 2 specify the interferometer and the observing date, respectively; Col. 3 reports the beam size (round) obtained from the geometrical average of the FWHM major and minor sizes of the naturally-weighted beam; Cols. 4 and 5 list the velocity resolution and the rms noise of the maser images (for channels devoid of signal). EVN observations were correlated with 1024 and 2048 spectral channels in 2004 and 2016, respectively.

2016 April 12 (code: RS002). We also reduced archival EVN observations obtained before the flare on 2004 November 6 (code: EL032). Both observations were conducted in phase-referencing mode by fast switching between the maser target (at a Doppler velocity of 5 km s^{-1}) and a strong (C-band flux >0.1 Jy) reference position calibrator, J0613+1708 (for exp. EL032) and J0603+1742 (for exp. RS002). Left and right circular polarizations were observed with two (EL032) and eight (RS002) baseband converters (BBC), each BBC being 2 MHz wide. The EL032 and RS002 experiments were processed at the correlator of the Joint Institute for VLBI in Europe (JIVE) using an averaging time of 0.5 s and 2 s, respectively. Data were analyzed with the NRAO[2] Astronomical Image Processing System (AIPS) following the VLBI spectral line procedures. Absolute positions of the CH_3OH maser spots are registered with an accuracy of about ± 1 mas at each epoch. Additional information on the EVN observations is summarized in Table 1.

2.2. JVLA continuum and 6.7 GHz CH_3OH maser

We observed the C-band (4–8 GHz) continuum and 6.7 GHz CH_3OH maser emission in NIRS 3 with the JVLA of the NRAO using both the B- and A-Array configurations (code: 16A-424). Table 1 reports the main observational parameters. For high-sensitivity continuum observations, we employed the three-bit samplers, observing dual polarization across the maximum receiver bandwidth of 4 GHz. A narrow spectral unit of 4 MHz was centered at the rest frequency of the 6.7 GHz maser transition and correlated with 1664 channels. 3C48 was observed as flux density, bandpass, and delay calibrator. As a complex gain calibrator we used J0534+1927, which has a correlated flux of ≈1 Jy and an angular separation of about 7° from the target maser. Data were reduced with the Common Astronomy Software Applications package (CASA v 4.3.1) making use of the JVLA pipeline. Mainly because of radio frequency interferences, which severely affect the C band, about 30% of the original data was flagged. We performed self-calibration (both in phase and amplitude) on the strongest maser channel at an LSR velocity of 6.4 km s^{-1} and applied these solutions to all maser channels before imaging. Based on a cross match between the JVLA and EVN maser maps during the outburst phase, we estimate an astrometric accuracy of ±50 mas for the JVLA dataset.

[2] The National Radio Astronomy Observatory (NRAO) is a facility of the National Science Foundation operated under cooperative agreement by Associated Universities, Inc.

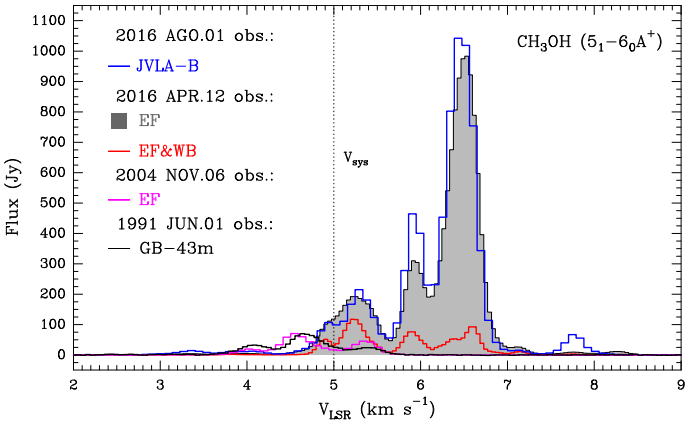

Fig. 1. Comparison of 6.7 GHz CH_3OH maser spectra obtained toward NIRS 3. Two single-dish pre-burst spectra obtained with the Green Bank (GB–43 m, black) and Effelsberg (EF, magenta) antennas are compared with the emission detected during the outburst phase at three different baselines: an EF total-power (filled histogram), a cross-power (red) of the EF and Westerbork (WB) baseline (~250 km), and a synthesized VLA spectrum (blue) obtained in the B configuration (maximum baseline of 11 km). The legend on the left side reports the observing dates. The dotted vertical line indicates the systemic velocity (V_{sys}) of the source S255-SMA1 from Zinchenko et al. (2015).

3. Results

Figure 1 compares 6.7 GHz maser spectra observed both before and during the NIR burst, and obtained with both single-dishes and interferometers. The Effelsberg spectra clearly show that new intense spectral features appeared during the burst at $V_{LSR} \geq 6$ km s^{-1} (hereafter, the flare emission), redshifted with respect to the pre-burst main spectral lines. On the other hand, pre-burst spectra show no significant variations since the first detection of this maser by Menten (1991). Figure 1 shows that the flare emission is heavily resolved on even the shortest EVN baselines between Effelsberg and Westerbork, which recover only ≈10% of the peak flux. About 3.5 months after the EVN run, JVLA B-Array observations recover the entire Effelsberg flux within a beam of about 1″, indicating a substantial time stability in the outbursting maser spectrum. The only notable change occurs in the secondary peak at V_{LSR} of 5.9 km s^{-1}, which shows a further increase by about 50%.

Figure 2 shows the spatial and V_{LSR} distribution of individual 6.7 GHz CH_3OH maser centers observed with the EVN before (triangles) and after (circles) the burst. The gray-scale image represents the velocity-integrated emission of the 6.7 GHz masers recovered with the JVLA A-Array. The 5 GHz continuum emission in the region (red contours) pinpoints the position of the massive YSO NIRS 3. Pre-burst maser emission originates within a radius of 0.3″ from the massive YSO, and lies above the 5 GHz continuum emission. By comparing Figs. 1 and 2, we infer that the flare emission arises from a region twice as large as the pre-burst emission, with the brightest spectral feature ($V_{LSR} \approx 6.5$ km s^{-1}) located at the position of cluster A. Cluster A coincides in position and V_{LSR} with the redshifted side of the rotating envelope observed by Zinchenko et al. (2015, their Fig. 5) with the SMA in 2011. These pre-burst observations reveal a rich reservoir of CH_3OH molecules in the gas phase with a relative (to H_2) abundance of 10^{-6} at a temperature of 170 K, suitable for maser excitation. The richest pre-burst cluster ("P" in Fig. 2), located NW of the radio continuum peak, disappears during the outburst phase. The close correspondence between the maser emission in the EVN and JVLA A-Array maps suggests

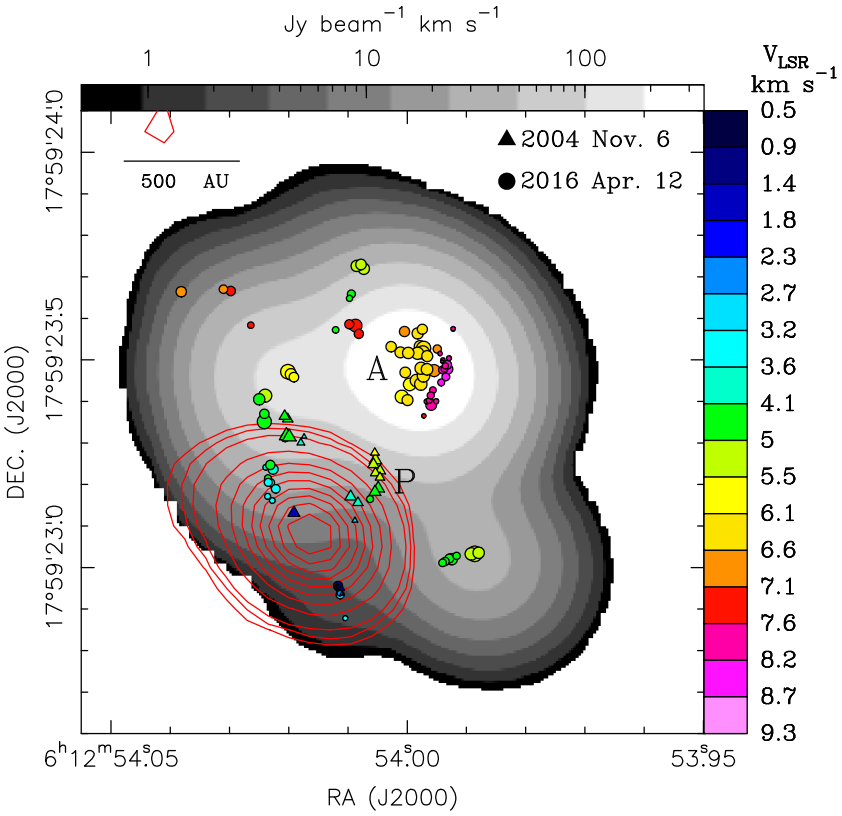

Fig. 2. Distribution of the 6.7 GHz CH_3OH masers toward NIRS 3. Circles and triangles represent maser spots before and after the outburst, respectively. Relative maser positions between the two epochs are accurate within a few mas. Note that the apparent motion of the 6.7 GHz CH_3OH masers in NIRS 3 between the two EVN epochs is negligible (Rygl et al. 2010). The symbol size varies logarithmically with the maser brightness, and colors indicate the maser V_{LSR} according to the right-hand scale. Letters "A" and "P" are used to label prominent maser clusters. The gray-scale image shows the velocity-integrated emission of the 6.7 GHz masers observed with the JVLA A-Array on 2016 October 15. The corresponding intensity scale is given at the top. The JVLA 5 GHz continuum emission is drawn with red contours. The rms noise of the image is 12 μJy beam^{-1}. Contour levels are 0.11, 0.15, and from 0.22 to 2 mJy beam^{-1} in steps of 0.22 mJy beam^{-1}. The synthesized beam of the continuum map is 0.″25 × 0.″24 at PA = 51°.

that no significant changes in maser positions occurred between 2016 April and October.

For the brightest maser channel at a V_{LSR} of 6.43 km s^{-1}, Fig. 3 presents a plot of the visibility amplitude as a function of the JVLA baseline length, after combining the A- and B-Array datasets. This plot shows that the flare emission at its spectral peak is slightly resolved by the JVLA observations. While on the shortest baselines the B-Array configuration recovers the entire Effelsberg flux (≈1000 Jy, see Fig. 1), about 10–15% of the single-dish flux is already missing on the longest baselines (<235 Kλ). This behavior is consistent with a source angular size of ≈0.″24. At the resolution of the A-Array configuration (for baselines >235 Kλ) the maser flux progressively decreases with increasing baseline length, following a profile that can be fitted with a more compact spatial structure of size ≈0.″1.

4. Discussion

In the following, we show that the radiation field triggered by the accretion burst excites a plateau of maser emission across a large portion of the redshifted envelope surrounding NIRS3 (between radii of 500–1000 AU). Throughout the wavelength range 20–30 μm that contains the pumping transitions of the 6.7 GHz maser line, the outburst flux from NIRS 3 exceeds the pre-burst level by a factor from ≈3 (at 20 μm) to ≈10 (at 30 μm; Caratti O Garatti et al. 2016; see Fig. 3). The 6.7 GHz maser burst was reported less than five months (November 2015) after the estimated beginning of the IR burst (June 2015; Caratti O Garatti et al. 2016). On this basis, it is reasonable to assume that the maser burst has been triggered by the IR burst. At a trigonometric distance of 1.8 kpc (Rygl et al. 2010; Burns et al. 2016), cluster A is projected more than 500 AU from the location of the high-mass YSO (identified by the radio continuum peak in Fig. 2). In order to produce a change in maser excitation conditions at position A, the triggering event has to propagate at a speed ≥0.02 c from the origin of the burst. This proves that the maser flare cannot be excited by a mechanical perturbation of the circumstellar medium, but must be triggered by the enhanced radiation field that is due to the accretion event.

Masers can operate in two different regimes. We indicate with T_m and τ the brightness temperature and the optical depth of the maser radiation. Weak masers are normally unsaturated, in which case $T_m = T_0\ e^{|\tau|}$, where T_0 is the brightness temperature of the background radiation amplified by the maser. At increasing intensity masers start to saturate, and in this regime, the brightness temperature grows only linearly with the optical depth, that is, $T_m \propto \tau$. In general, $|\tau| \propto P\ \eta\ l_m$, meaning that the maser optical depth is proportional to the total pump rate P to the maser levels, the pumping efficiency, η, and the amplification path, l_m. If the masers are radiatively pumped, P is proportional to the flux F_p of pumping photons incident on the masing gas.

In our case, from the ratio between the outburst on pre-burst luminosities, we find that F_p has increased by a factor ≈5. In 2016 April, during the burst, our EVN observations derived maser intensities in the range 0.1–100 Jy beam^{-1}, corresponding to brightness temperatures of 10^8–10^{11} K. Since pre-burst EVN 6.7 GHz observations did not detect emission at the same location of the flaring masers, pre-burst maser intensities should be < 50 mJy or, equivalently, $T_m < 5 \times 10^7$ K. Comparing the relatively small change in F_p (<10) with the large variation in maser intensity (more than 3–4 orders of magnitude), we can argue that most of the growth in maser intensity has occurred in a regime of non-saturation. In Appendix A, we estimate the brightness temperatures of both the maser saturation level, $T_s = 10^{10}$ K, and the background radiation, $T_0 \leq 50$ K. Based on these estimates, the maser gain, $G = e^{|\tau|}$, has to be in the range 10^7–10^9 to account for the outburst brightness of the unsaturated masers (10^8–10^{10} K). If F_p and $|\tau|$ increase by a factor ≈5 during the burst, the outburst maser gain should be approximately the

fifth power of the pre-burst gain. Thus $G \leq 10^2$ before the burst, corresponding to $|\tau| \leq 5$ and pre-burst brightness temperatures $\leq$5000 K. This is about four orders of magnitude below the EVN detection threshold, consistent with the non-detection of emission throughout the maser flare area by VLBI observations before the burst.

Figure 1 shows that the large majority (>90%) of the flux of the strongest peak of the Effelsberg 6.7 GHz maser spectrum, emerging from cluster A (see Fig. 2), is resolved out on the Effelsberg-Westerbork baseline. VLBI observations of the 6.7 GHz masers have presented many cases of spectral features that were heavily resolved even on the shortest baselines of the VLBI array (Minier et al. 2002), suggesting that 6.7 GHz CH_3OH masers have a core/halo structure, with core and halo diameters ranging in the intervals 2–20 AU and 10–300 AU, respectively. However, larger flux losses are generally observed for weaker spectral components, whereas most of the flux of the strongest peak is recovered. Instead, in NIRS 3 the reverse occurs, and Fig. 3 indeed proves that the spatial structure of the 6.7 GHz maser spectral peak is extended, with a size of up to 0.″24, or 430 AU, which is larger than the typical maser halos measured by Minier et al. (2002). Our EVN observations, filtering out spatial scales $\gtrsim$70 AU, resolve cluster A into a tight cluster of strong maser spots. These compact spots are just local peaks emerging from a continuous plateau of weaker 6.7 GHz maser emission. From Fig. 3, we estimate that the brightness temperature of this maser plateau is $\approx 5 \times 10^8$ K.

So far, our discussion has focused on the bursting maser emission. Now, we turn our attention to the main pre-burst cluster ("P", see Fig. 2). Since the 6.7 GHz maser spectrum toward NIRS 3 is approximately stable over a timescale of $\approx$13 yr before the burst (see Fig. 1), we can reasonably assume that the disappearance of cluster P is due to the accretion burst, and we discuss two possible ways of maser suppression: 1) UV photodissociation of CH_3OH, and 2) perturbation of the velocity coherent path. Figure 2 shows that cluster P is located at an average distance $R_P \approx 0.''2$, or 340 AU, from the YSO and has a size $D_P \approx 0.''14$, or 240 AU. Using the value of H_2 (number) density $n_{H_2} \sim 10^8$ cm^{-3}, as determined by Zinchenko et al. (2015) for the molecular envelope around NIRS 3, we estimate for cluster P an H_2 column density $N_{H_2} \approx 4 \times 10^{23}$ cm^{-2}, corresponding to a visual extinction $A_V \approx 400$ mag. In Appendix B, we find that the threshold in visual extinction needed to shield CH_3OH from photodissociation in cluster P is $A_V \gtrsim 7$ mag. With the caveat of our simplistic assumptions of homogeneous density distribution for the molecular envelope and isotropic radiation from the YSO, we therefore consider it unlikely that UV photodissociation induced by the accretion burst is the main cause for the disappearance of this cluster of 6.7 GHz masers.

A line-of-sight velocity coherence over a long path is needed for maser amplification. The change in velocity, ΔV, that is due to radiation pressure on the maser cluster P can be estimated with the expression $\Delta V = L\, t\, \frac{\Omega_P}{4\pi M_P c}$, where c is the speed of light, L is the outburst luminosity of NIRS 3, t is the time over which the mechanism is at work (i.e., the duration of the burst), M_P is the mass of the molecular clump harboring the maser cluster P, and Ω_P is the solid angle subtended by cluster P at the YSO position. Using $R_P \approx 340$ AU and $D_P \approx 240$ AU for the radial distance and the size of cluster P, respectively, and a density $n_{H_2} \sim 10^8$ cm^{-3}, we derive $\Omega_P \approx 0.4$ sterad and $M_P \approx 4 \times 10^{-3}\ M_\odot$. With $L = 1.6 \times 10^5\ L_\odot$ and $t \approx 1$ yr (approximately the time elapsed from the onset of the burst in June 2015 and the EVN observations in April 2016), we estimate

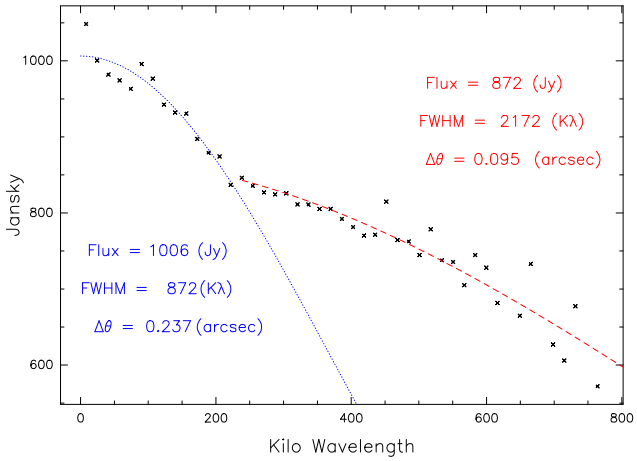

Fig. 3. Visibility amplitude vs. JVLA baseline length for the brightest maser channel (at $V_{LSR} = 6.43$ km s^{-1}). The blue dotted and red dashed lines show the Gaussian fits to the amplitude profile using only data with baseline lengths lower and higher than 235 Kλ, respectively, which is the maximum baseline sampled with the B-Array. The amplitude and FWHM size of the fitted Gaussians are reported with consistent colors.

$\Delta V \approx 0.03$ km s^{-1}. This value, calculated using the whole clump mass, is probably a lower limit, since the whole radiative flux could be intercepted only by the portion of the clump closer to the YSO. Thus, we consider it plausible that radiative pressure, over a timescale of $\approx$1 yr, could have produced a velocity change comparable with the 6.7 GHz maser line width of 0.1–0.2 km s^{-1} along a sizable fraction of the maser path length. For unsaturated operation, this effect could have drastically reduced the maser intensities in cluster P. Repeating the same calculation for cluster A with a distance $R_A \approx 0.''45$ (800 AU) and a size $D_A \approx 0.''240$ (430 AU), we find $\Delta V \approx 0.002$ km s^{-1}. This is an order of magnitude lower than the value estimated for cluster P, which might explain why radiation pressure does not destroy the velocity coherence of the 6.7 GHz masers in cluster A.

Acknowledgements. A.S. gratefully acknowledges financial support by the Deutsche Forschungsgemeinschaft (DFG) Priority Program 1573. M.C.W. and A.C.oG. were supported by Science Foundation Ireland, grant 13/ERC/I2907.

References

Burns, R. A., Handa, T., Nagayama, T., Sunada, K., & Omodaka, T. 2016, MNRAS, 460, 283
Caratti O Garatti, A., Stecklum, B., Garcia Lopez, R., et al. 2016, Nature Phys., 13, 276
Draine, B. T. 2011, Physics of the Interstellar and Intergalactic Medium (Princeton University Press)
Elitzur, M. 1992, Astronomical masers, Astrophys. Space Sci. Lib., 170,
Fujisawa, K., Yonekura, Y., Sugiyama, K., et al. 2015, ATel, 8286, 1
Goedhart, S., Gaylard, M. J., & van der Walt, D. J. 2004, MNRAS, 355, 553
Heays, A. N., Bosman, A. D., & van Dishoeck, E. F. 2017, A&A, in press, DOI: 10.1051/0004-6361/201628742
Menten, K. M. 1991, ApJ, 380, L75
Minier, V., Booth, R. S., & Conway, J. E. 2002, A&A, 383, 614
Moscadelli, L., Menten, K. M., Walmsley, C. M., & Reid, M. J. 2003, ApJ, 583, 776
Moscadelli, L., Sanna, A., & Goddi, C. 2011, A&A, 536, A38
Rygl, K. L. J., Brunthaler, A., Reid, M. J., et al. 2010, A&A, 511, A2
Sanna, A., Moscadelli, L., Cesaroni, R., et al. 2010, A&A, 517, A71
Sobolev, A. M., Cragg, D. M., & Godfrey, P. D. 1997, A&A, 324, 211
Stecklum, B., Caratti o Garatti, A., Cardenas, M. C., et al. 2016, ATel, 8732
Zinchenko, I., Liu, S.-Y., Su, Y.-N., et al. 2015, ApJ, 810, 10

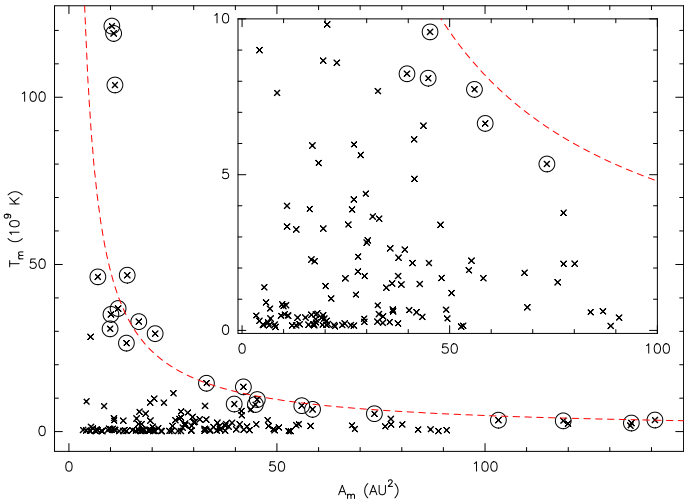

Fig. A.1. Brightness temperature of the spots (in units of 10^9 K) vs. the deconvolved sky-projected spot area (in AU^2). The spot area is defined as $A_m = (\pi/4)\,a\,b$, a and b being the deconvolved FWHM along the major and minor axes, respectively. Circles with crosses indicate the spots with $T_m A_m \geq 300 \times 10^9$ K AU^2. The red dashed line gives the best hyperbolic fit to these points, $T_m \propto 1/A_m$. The inset shows an enlargement of the region with $T_m \leq 10^{10}$ K.

Appendix A: Determination of saturation and background brightness temperatures

In order to evaluate the maser optical depth, we need to estimate the brightness temperatures of saturation and background radiation. To estimate the saturation level we employ the method by Moscadelli et al. (2003), based on plots of the maser brightness temperature, T_m, versus the emission area, A_m. Since the flux of saturated masers, expressed by the product $T_m A_m$, approaches but cannot exceed the flux of the pumping photons, all saturated masers lie close to a curve $T_m A_m = K$, with K being a constant. Figure A.1 shows that all the spots with a sufficiently high value of $T_m A_m$ ($\geq 300 \times 10^9$ K AU^2) lie close to an upper envelope, well fit with the hyperbola $T_m A_m = 480 \times 10^9$ K AU^2. From the same plot we can evaluate that while all the masers with $T_m \geq 10^{10}$ K are saturated, the large majority of those with $T_m \leq 10^{10}$ K are still unsaturated. Therefore we can take as a threshold for saturation $T_s = 10^{10}$ K. Maser theory predicts that the line width of the spectral profile of unsaturated masers is subthermal and that the maser line width relaxes to the thermal value only after the threshold of saturation is crossed. As a further check of the saturation condition, we also determined the FWHM line width of the masers by fitting a Gaussian profile to the spectra of individual maser spots. We find that it varies in the small range 0.18 ± 0.05 km s^{-1}. This value is significantly lower than the thermal line width ≥ 0.43 km s^{-1} expected for a kinetic temperature ≥ 150 K (as derived by Zinchenko et al. 2015, in the molecular envelope surrounding NIRS 3), and it supports our conclusion that most of the outbursting masers are still unsaturated.

We identify three possible contributions to the maser background radiation T_0: 1) spontaneous emission, 2) dust emission, and 3) ionized gas emission. For unsaturated masers, the brightness temperature of spontaneous emission is given by $\frac{h\nu_0}{k}\frac{1+\eta}{2\eta}$ (Elitzur 1992, Eqs. (2.3.28) and (4.2.11)), where h and k are the Planck and Boltzmann constants, respectively, and ν_0 is the maser line rest frequency. For values of η in the range 0.1−1, spontaneous emission always contributes ≤ 2 K. Since dust emission is optically thin at centimeter wavelengths, its brightness temperature is $\approx T_d\,\tau_d$, where T_d and τ_d are the kinetic temperature and the optical depth of the dust, respectively. Using $T_d \leq 200$ K (Zinchenko et al. 2015) and $\tau_d \ll 0.1$, we estimate a dust contribution $\ll 20$ K. Our C-band VLA A-Array observations do not detect free-free emission toward cluster A, where the most intense 6.7 GHz masers are found. The 3σ continuum detection threshold of 36 μJy beam^{-1} corresponds to a brightness temperature of 16 K. Adding the contributions of the spontaneous, dust and free-free emissions, we derive $T_0 \leq 50$ K.

Appendix B: Photodissociation of the CH_3OH molecule in cluster P

In the following, we wish to evaluate the threshold in visual extinction to shield CH_3OH molecules inside cluster P from the UV flux produced by the accretion burst in NIRS 3. The UV energy density, E_{UV}, inside cluster P can be estimated with the expression

$$E_{UV} = f_{UV}\,\frac{L}{c(R_P)^2} \tag{B.1}$$

where c is the speed of light, $R_P = 340$ AU is the distance of cluster P from NIRS 3, $L = 1.6 \times 10^5\ L_\odot$ is the outburst luminosity of the YSO, and f_{UV} is the fraction of that luminosity in photons with wavelength ≤ 2800 Å, which is the photodissociation threshold of CH_3OH (Heays et al. 2017). We find $E_{UV} = f_{UV}\ 8 \times 10^{-4}$ erg cm^{-3}. A probable range for f_{UV} is $0.1 \leq f_{UV} \leq 1$, which implies $8\,10^{-5} \leq E_{UV} \leq 8 \times 10^{-4}$ erg cm^{-3}. This value of the energy density is a factor 1.6×10^9–1.6×10^{10} higher than the average field in the interstellar medium (ISM) of 5×10^{-14} erg cm^{-3} (Draine 2011). The photodissociation rate of CH_3OH within a molecular clump exposed to the average ISM field is estimated to be $1.4 \times 10^{-9}\ \exp(-2.76\,A_V)$ molecule^{-1} s^{-1} (Heays et al. 2017), where A_V is the visual extinction of the clump. By scaling this value proportionally with the energy density of the radiation field, we can estimate that CH_3OH inside cluster P is photodissociated at a rate of $\sim 10\ \exp(-2.76\,A_V)$ s^{-1} molecule^{-1} s^{-1}. Based on this rate, we derive that a value of $A_V \geq 7$ mag can be enough to efficiently shield all the CH_3OH molecules within cluster P over the timescale of ≈ 1 yr between the onset of the burst (June 2015) and the EVN observations (April 2016).